Supporting Information for

Assessing Conditions Favoring the Survival of African Dust-Borne Microorganisms during Long-Range Transport across the Tropical Atlantic

Ali Hossein Mardi[a], Miguel Ricardo A. Hilario[b], Regina Hanlon[c], Cristina Gonzalez-Martin[d], David Schmale[c], Armin Sorooshian[b,e], Hosein Foroutan[a,*]

a) Department of Civil and Environmental Engineering, Virginia Tech, Blacksburg, Virginia, USA
b) Department of Hydrology and Atmospheric Sciences, University of Arizona, Tucson, Arizona, USA
c) School of Plant and Environmental Sciences, Virginia Tech, Blacksburg, Virginia, USA
d) Instituto Universitario de Enfermedades Tropicales y Salud Pública de Canarias, Universidad de La Laguna, San Cristóbal de La Laguna, Spain
e) Department of Chemical and Environmental Engineering, University of Arizona, Tucson, Arizona, USA

*Corresponding author: Hosein Foroutan (hosein@vt.edu)

Contents of this file

Section S1-S2, Tables S1-S3, Figures S1-S7

S1. Interannual Variations in the Equivalent Center of Dust Emission

Focusing solely on the long-term seasonal averages or total emission maps might obscure the interannual variations in the location of dust sources impacting each receptor region the most. For this reason, we had a closer look at the interannual variations in the equivalent center of dust emission for each receptor region. The latitude and longitude for the equivalent dust emission center is calculated based on the following formulas:

$$Lat = \frac{\sum_{i=1}^{n} E_i Lat_i}{\sum_{i=1}^{n} E_i} \quad \text{(S1a)}$$

$$Lon = \frac{\sum_{i=1}^{n} E_i Lon_i}{\sum_{i=1}^{n} E_i} \quad \text{(S1b)}$$

In equations (S1a,b), n represents the number of dust-emitting pixels on each panel of total seasonal dust emission maps for a certain year, E_i represents the emission associated with a certain pixel, and Lat_i and Lon_i are the latitude and longitude of that pixel, respectively. The seasonal location of the equivalent dust emission centers for trajectories impacting each receptor region are shown in Figure S1. Except for trajectories reaching US-CARIB in the peak season of June - August, the location for the center of emission experienced notable spatial variation throughout the years, moving along a diagonal line between south-central and north-western parts of North African desertified regions, extended from southwestern Niger and along the diagonal border of Algeria, Mali, and Mauritania. Almost all of the interannual spatial variation in the center of emissions happens due to shifting between two dominant dust emitting regions along this line, connecting the western emission sources and the Bodélé depression in Chad. This pattern denotes the profound role of these two regions in driving the equivalent dust emission source. The significant influence of these two regions has been frequently discussed in the literature. Relevant to this work are the results from a study by Yu et al.[1], who discussed the role of two

dominant dust emitting regions of Bodélé and El Djouf over the course of 2005 – 2017 in supplementing westward receptor regions with nutrients. However, there was no discussion of interannual variation in the extent of emissions from each of these sources. It is worth noting that, to the best of our knowledge, the interannual trend over such a prolonged period and considering all potential North African dust sources that could reach the western tropical Atlantic Ocean, have not been analyzed with details before. A relevant study to consider is Doherty et al.[2], which explored the correlation between interannual variations in Barbados dust load and the latitudinal displacement of the ITCZ over a 38-year period. In their study, it was concluded that southward and eastward movement of the ITCZ leads to increased quantity of mineral dust load over Barbados due to inclusion of Bodélé region among contributing source areas. As another example, Wagner et al.[3] compared the emission source between 2007 and 2008 and mentioned 2008 as the year with the greatest impact from the Bodélé depression. We do not have the data from 2007 but our results demonstrate the heaviest impact from Bodélé in 2008, from December to February. In a similar study, Barkley et al.[4] studied the North African dust emissions during 2014 and 2016 and captured the heavy dust emission activity from Bodélé that dragged the center of emission towards the south-central region. Similarly, in our results, the dust emission center is shifted toward the central regions in 2016, which denotes a higher impact from Bodélé in that year. The seasonal shift in the location of dust emitting sources have also been reported in numerous other studies for a wide variety of receptor regions[5, 6]. In a study by Rodríguez et al.[7], the difference between the intensity of the summertime high system over the Sahara and tropical low at 850 mb (~ 1500 m) is denoted as one of the strong governing factors impacting African summertime dust emissions. The study of dust emission mechanisms by Caton Harrison et al.[8] also unveils cold pool activity, initiated around the Mali-Niger-Algeria border triple point, as the primary driver of summertime emissions. Long-term variations in the equivalent center of dust emissions can also be impacted by ongoing variations in greater scale meteorology over the tropical Atlantic Ocean. In a related study, Li et al.[9] analyze the long-term impact of deforestation in tropics on African dust emissions and reports a shift in the location of peak surface dust concentrations toward the south as a result of a change in the albedo of tropics, induced by deforestation. This interconnectedness of dust emissions to the greater variations in the governing circulations' regimes over the Atlantic Ocean have been subject of numerous publications, especially given the role of convective systems in creating large plumes of dust over Africa[10] (and references therein). This motivates the need for future studies in this field, which are beyond the scope of the current study.

Another observation is the small variation in the equivalent dust emission source location for trajectories reaching US-CARIB during the peak of June to August. This is in contrast to the variation observed for AMZN during its peak of December to February. This finding should be considered in the light of existing debate about the specific sources of dust reaching the Amazon basin, which is a result of lacking conclusive evidence determining the true source of Amazonian dust. Some early analysis of remote sensing retrievals suggests that up to 40% of Amazonian dust is sourced from the Bodélé depression[11]. However, further analysis of surface sediments and geochemical traits in dust samples collected from the Amazon basin is inconsistent with the dominant role of Bodélé depression in supplying dust to Amazon basin[12]. These inconsistencies are mainly rooted in short time-spans during which the studies are conducted and hence, a long-term interannual analysis of dust sources can further clarify the role of the Bodélé depression in trans-Atlantic dust transport[1] to receptor regions on the western side of Atlantic Ocean. Additionally, dividing the receptor region into smaller sub-domains could result in a more detailed and resolved answer about the origin of dust aerosols impacting the Western Central Atlantic Ocean receptor regions.

Current modeling results when combined with trajectory analysis are in accordance with findings of previous studies[1, 13, 14], which suggest that emissions from the Bodélé depression do not have as profound of an impact on the US-CARIB region as compared to AMZN. Additionally, it should be noted that based on these results, even though Bodélé plays an integral role in dust emissions impacting the AMZN, it is not the sole source contributing to the annual dust load and by taking into the account the amount of dust intercepted by wet deposition mechanisms[1], the amount of dust contribution diminishes significantly. However, these results are notable as distinct geographical regions will potentially emit distinct taxa of microorganisms[15] and regardless of the portion of dust plumes that reaches the Amazon region, based solely on the origin of emissions, higher interannual diversity is expected for emissions impacting the AMZN receptor region.

S2. Forward/Backward Evaluation of HYSPLIT Model

There are several uncertainties associated with HYSPLIT trajectories rooted in field data source used for calculation of trajectories . Examples of errors associated with data field include data grid resolution, misrepresentation of turbulence, interpolation errors, miscalculation of vertical wind motion, and inaccurate representation of trajectory location due to scale mismatch at each step[16, 17]. Despite the various potential sources of error mentioned, when provided inputs that closely

resemble real-world conditions, the HYSPLIT model demonstrates a high degree of certainty[18], with better resemblance for forward mode trajectories as compared to backward mode[19]. However, it should be noted over long distances, the level of uncertainty will increase considerably[20] and this motivates analysis of uncertainty for HYSPLIT trajectories. The large number of trajectories in a run ensemble can improve the certainty of outcomes by cancellation of random errors[21]. Additionally, we performed a forward/backward evaluation of HYSPLIT trajectory based on the method proposed by Fuelberg et al.[22] to further analyze the accuracy of HYSPLIT model runs over long distances and periods of time.

Comparing the number of steps between the forward and backward trajectories reveals a mismatch between the number of steps in backward vs forward mode (Figure S5). This can be attributed to the early termination of backward trajectories due to HYSPLIT internal model properties. An example of such properties is the maximum altitude defined for the model, which leads to the termination of the model, whenever trajectories reach it. To address this issue, trajectory pairs with similar number of steps in both forward and backward mode are compared as justified pairs, versus the non-justified pairs with possibly different number of steps in forward and backward mode. From a total of 2491 pairs for US-CARIB sub-domain, 1724 pairs have the same number of steps in both forward and backward mode. For the AMZN sub-domain, the percentage of remaining justified pairs is slightly higher with 1046 trajectory pairs of a total of 1387 (Table S3). Comparing the beginning longitude of forward trajectories with the ending point of backward ones, the root mean square error (RMSE) of 11.30° and 11.20° are observed for unjustified pairs of US-CARIB and AMZN, respectively. A similar comparison for the latitudes reveals smaller discrepancies in the latitudinal direction with RMSE values of 4.50° and 5.87°, respectively. Higher longitudinal errors are partly due to zonal nature of prevailing wind flow over the tropical Atlantic region, which leads to a greater displacement of backward trajectories ending point as a result of a change in the number of backward steps. The r2 values range between 0.26 to 0.49 for both parameters and regions. Removing the pairs with a different number of steps enhances the correlations (Table S3) with r2 values ranging from 0.65 to 0.99. For unjustified pairs, the average ending altitudes were 540 ± 619 m and 668 ± 738 m, for US-CARIB and AMZN, respectively. Similarly, removing the pairs with unequal number of steps drags the averages closer to the initial 300 m beginning point and decreases the standard deviation values. The highest improvement is observed for US-CARIB justified pairs with mean ending altitude of 313 ± 184 m, closely resembling the initial 300 m altitude. Enhancements are not as evident for AMZN pairs with 522 ± 569 m average ending altitudes after justification of pairs.

Among the meteorological parameters, mean RH and ambient temperature along the trajectories demonstrate highest correlations between the forward and backward mode with r^2 values ranging from 0.79 to 0.86. The high correlation can be attributed to the high spatial co-variability of these parameters which make them closely related over adjacent pixels of large swaths of area. The same cannot be said for the solar flux with unjustified r^2 values of 0.31 and 0.68 for US-CARIB and AMZN, respectively. The low correlation observed for US-CARIB is mainly due to a series of outlier pairs which exists, even after the justification of pairs based on the number of steps (figure S6, e and f) with r^2 values not reaching above the 0.51 level. However, for the AMZN pairs, r^2 values enhanced to 0.96 after the justification of the pairs. Additionally, downward solar fluxes are highly dependent on the cloud coverage which varies drastically from one pixel to another and leads to a lesser spatial co-variability as compared to RH and ambient temperature. Overall, 69 and 75% of pairs did not require any justification for US-CARIB and AMZN, respectively. For these pairs (Figure S6 and S7), initial coordination, altitude and meteorological parameters along the trajectories demonstrate high correlations between the forward and backward trajectories indicating their trustworthiness for a long-term statistical analysis.

Table S1. The seasonal average latitude and altitude of trajectories impacting each receptor region for different seasons.

		Dec.-Feb.	Mar.-May	Jun.-Aug.	Sept.-Nov.
Latitude (°N)	US-CARIB	14.2	11.9	17.5	14.9
	AMZN	9.6	9.2	11.5	9.8
Altitude (m)	US-CARIB	850	1712	1639	1142
	AMZN	663	1462	1940	1118

Table S2. The average travel time of trajectories (hr) intruding each receptor region for different seasons.

	Dec.-Feb.	Mar.-May	Jun.-Aug.	Sept.-Nov.
US-CARIB	251	280	270	282
AMZN	239	280	286	281

Table S3. The root mean square error (RMSE) and correlation coefficient (r^2) for statistical comparison of forward HYSPLIT trajectories to the backward trajectories initiated from the point of arrival to the receptor regions and continued for a similar number of steps. As all forward trajectories are initiated from a fixed 300 m altitude without any variations, the r^2 values would be meaningless for comparison of the altitudes and instead mean ± standard deviations are reported. The term “justified” ("unjustified”) refers to trajectory pairs with the same (differing) number of steps in forward and backward mode.

		US-CARIB		AMZN	
		Unjustified	Justified	Unjustified	Justified
Number of pairs		2491	1724	1387	1046
Number of steps	r^2	0.27	1.00	0.55	1.00
	RMSE	63.59	0.00	58.83	0.00
Latitude (°)	r^2	0.30	0.65	0.26	0.80
	RMSE	4.50	0.95	5.87	1.86
Longitude (°)	r^2	0.49	0.99	0.35	0.89
	RMSE	11.30	0.77	11.20	2.68
Altitude (m)	mean ± Stdv	540 ± 619	313 ± 184	668 ± 738	522 ± 569
	RMSE	619	184	738	569
Mean solar flux ($W\ m^{-2}$)	r^2	0.31	0.51	0.68	0.96
	RMSE	38.38	25.72	23.39	6.75
Mean ambient temperature (K)	r^2	0.79	0.99	0.81	0.97
	RMSE	5.77	0.87	2.09	0.57
Mean RH (%)	r^2	0.86	1.00	0.86	0.99
	RMSE	1.84	0.22	4.36	1.16

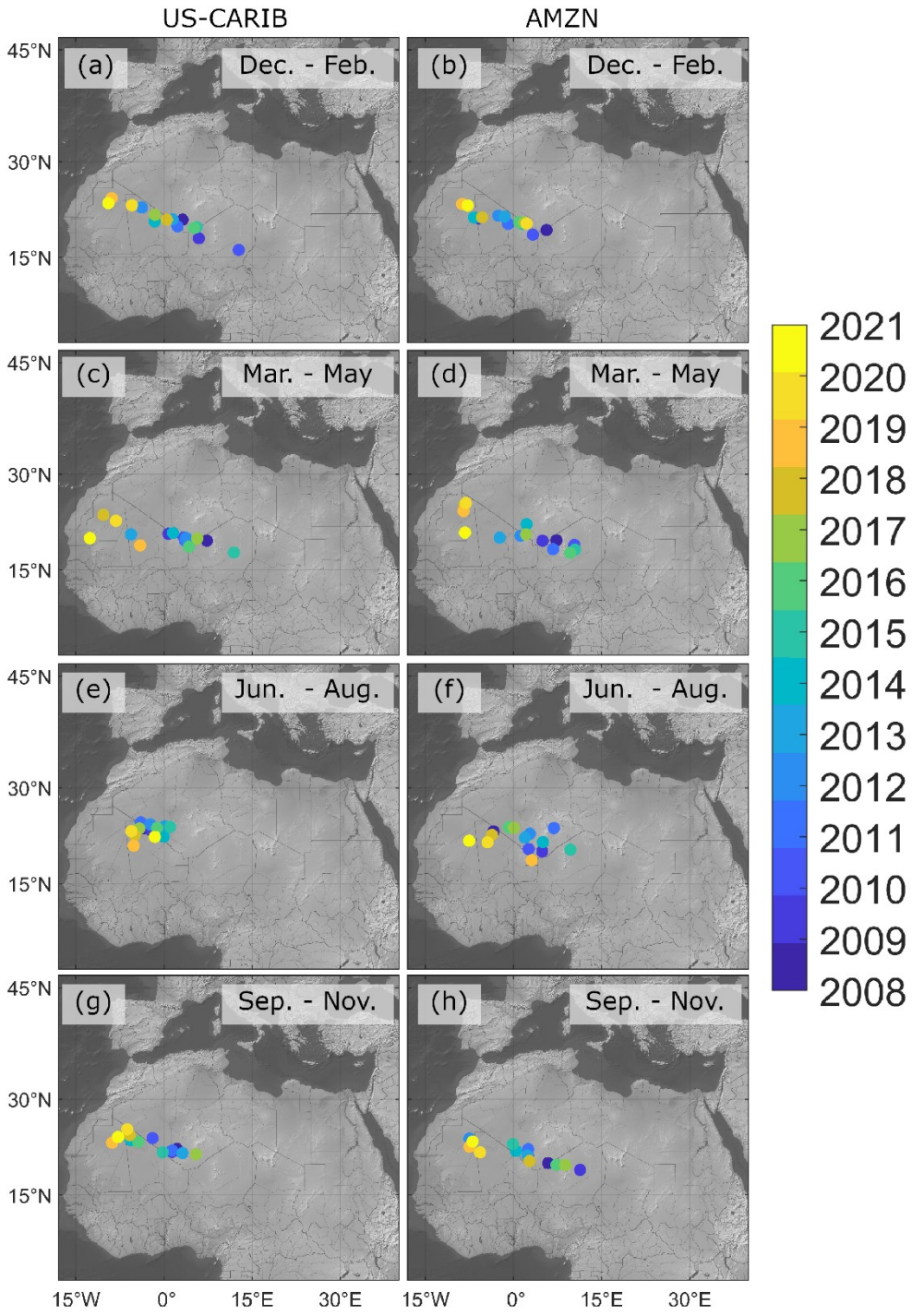

Figure S1. The seasonal location of the equivalent dust emission centers during December – February, March – May, June – August, and September – November, for trajectories impacting each receptor region. Panels a, c, e, and g belong to the US-CARIB and panels b, d, f, and h belong to AMZN region. Circles are color coded based on the year they belong to.

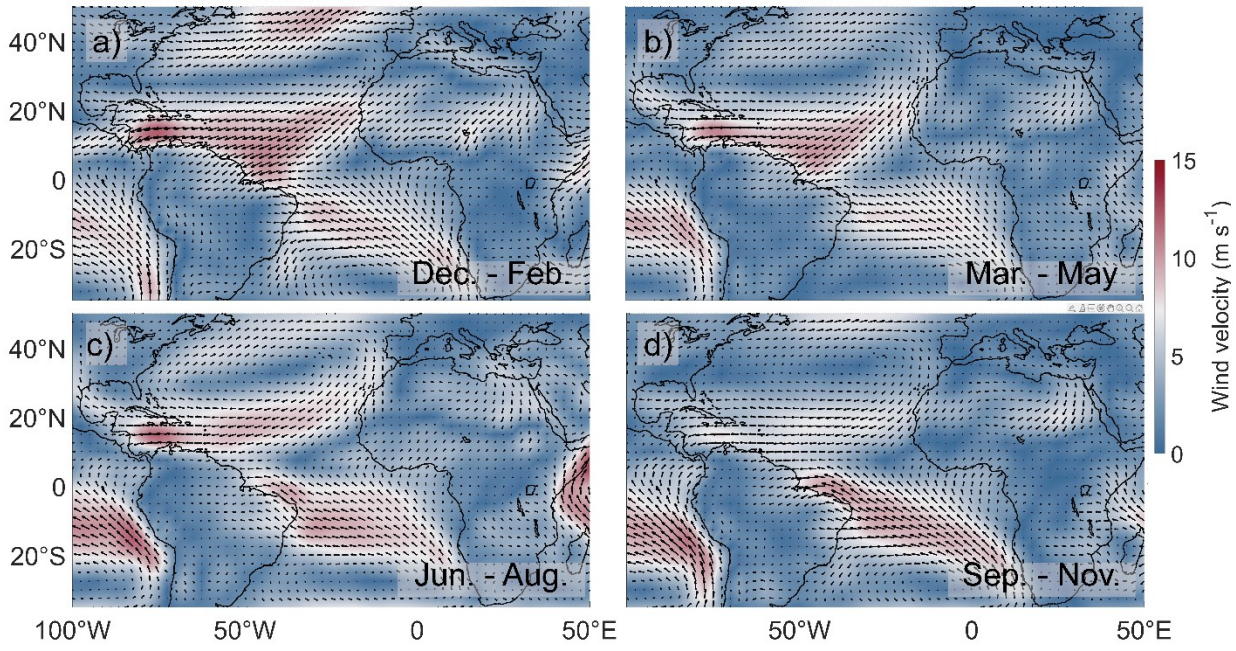

Figure S2. Mean seasonal direction and wind velocity over tropical Atlantic Ocean and neighboring regions averaged for pressure levels of 1000 – 850 mb, over the period of 2008 – 2021.

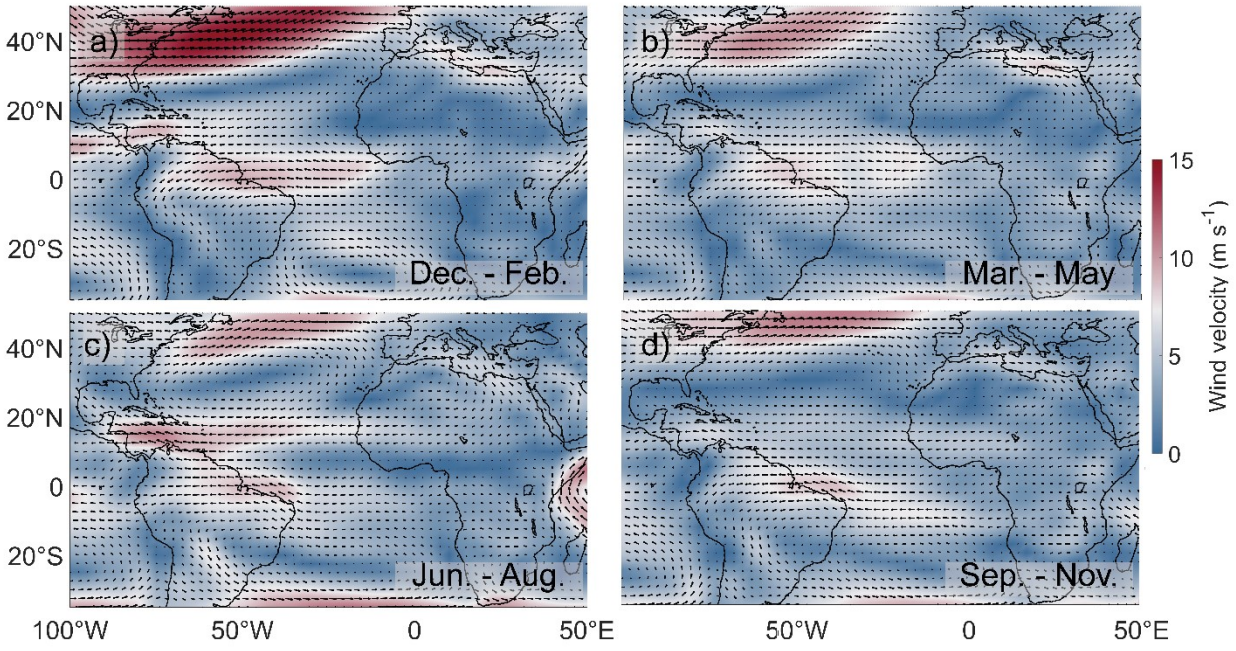

Figure S3. Same as Figure S1, but averaged for pressure levels of 850 – 650 mb.

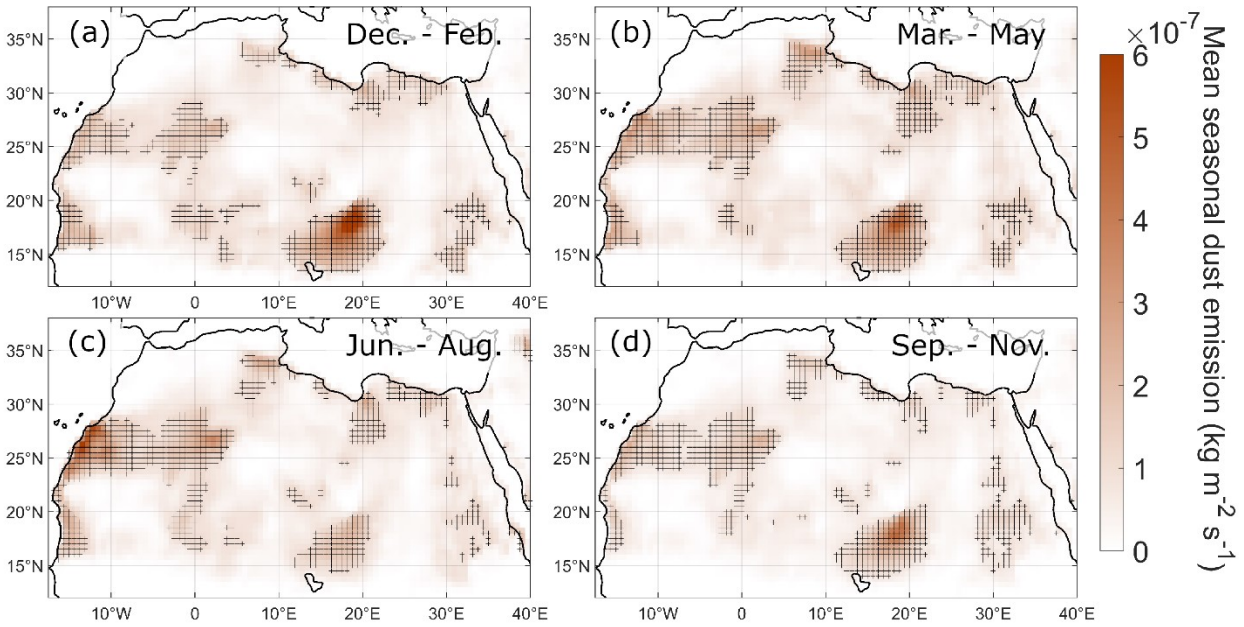

Figure S4. Mean seasonal dust emission values for 2008 – 2021 from arid regions of northern Africa. Hashed areas denote pixels with mean seasonal dust emission values greater than the 80th percentile on a Gamma function cumulative distribution assigned to the pixels of each season.

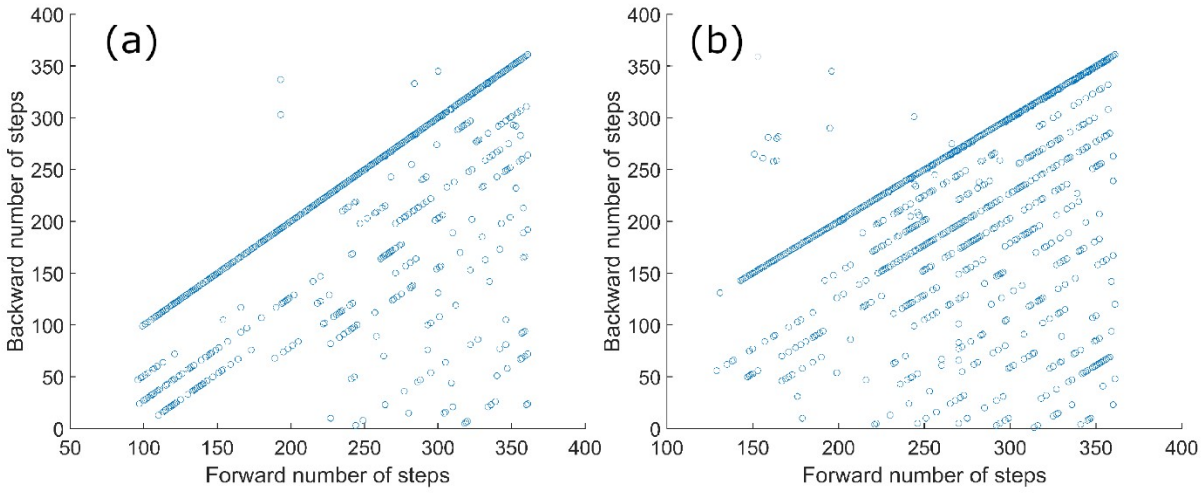

Figure S5. Scatterplot between the number of steps for the forward trajectories from the original run and the corresponding backward trajectories run from the point trajectories have entered each receptor sub-domain. Panels (a) and (b) represent trajectories reaching the US-CARIB and AMZN regions, respectively.

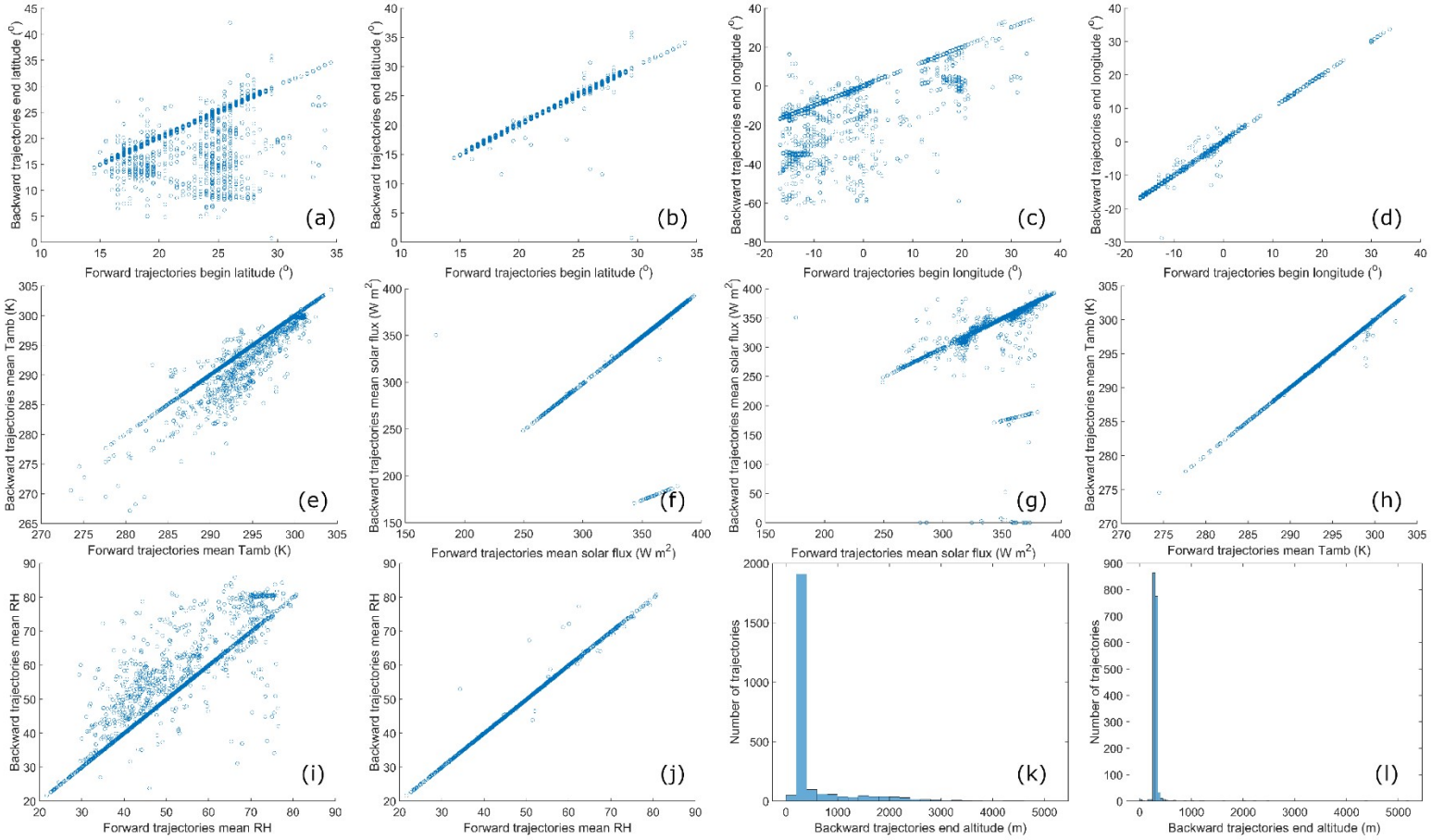

Figure S6. Scatterplot between select parameters of forward trajectories reaching the US-CARIB sub-domain during 2021 and their corresponding backward trajectory. Compared parameters include latitude (a and b), and longitude (c and d) at the beginning of the forward trajectories as compared to the ending points of backward trajectories. Additionally, average solar flux (e and f), ambient temperature (g and h), and RH (i and j) are compared. For the ending altitude of backward

trajectories, the histograms are shown (k and l). Panels b, d, f, h, j, and l belong to a group of justified pairs where the number of steps is equal in forward and backward trajectories.

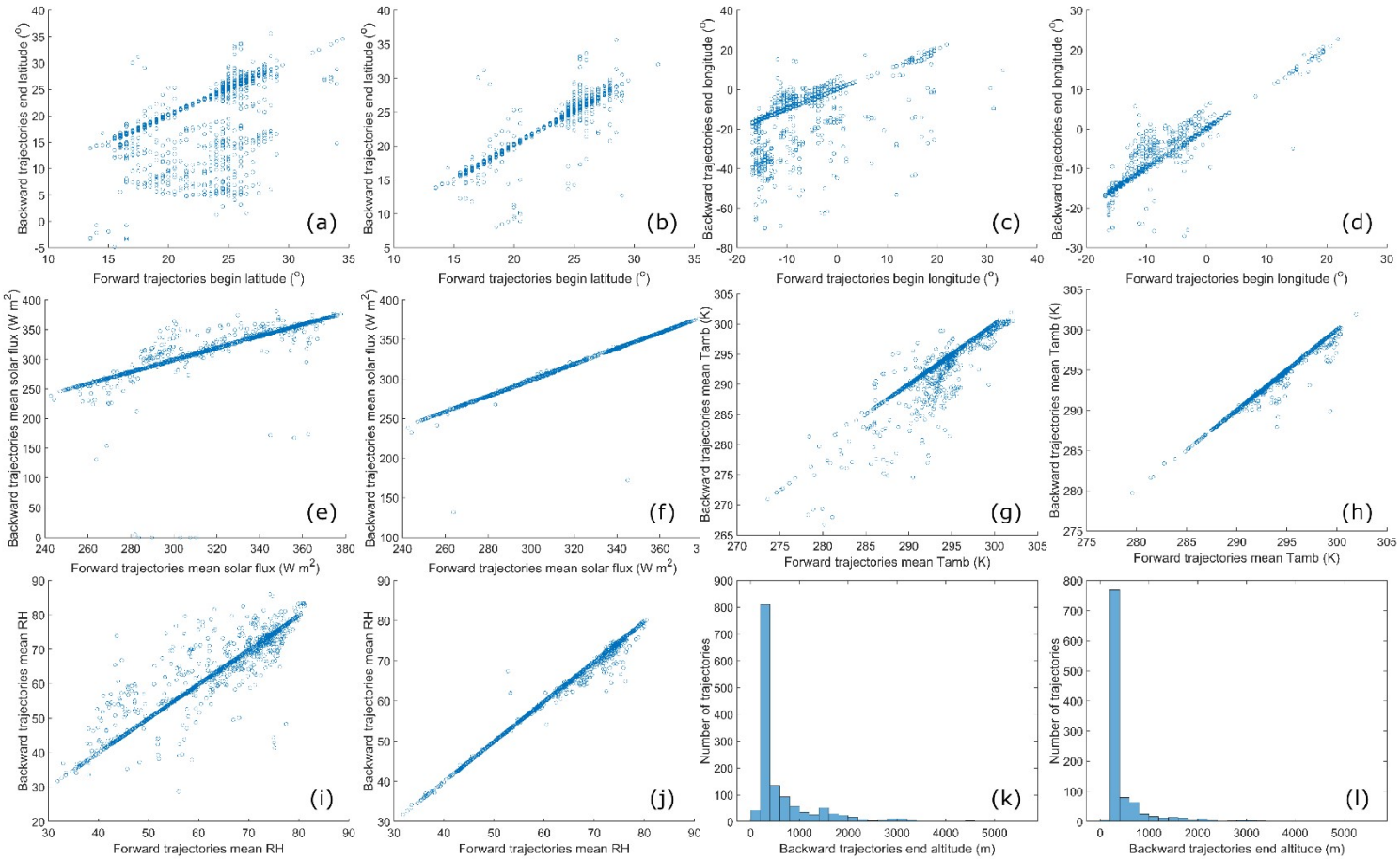

Figure S7. Same as Figure S3, except for the AMZN sub-domain.

Reference

1. Y. Yu, O. V. Kalashnikova, M. J. Garay, H. Lee, M. Notaro, J. R. Campbell, J. Marquis, P. Ginoux and G. S. Okin, Disproving the Bodélé depression as the primary source of dust fertilizing the Amazon Rainforest, *Geophysical Research Letters*, 2020, **47**, e2020GL088020.
2. O. Doherty, N. Riemer and S. Hameed, Control of Saharan mineral dust transport to Barbados in winter by the Intertropical Convergence Zone over West Africa, *Journal of Geophysical Research: Atmospheres*, 2012, **117**.
3. R. Wagner, K. Schepanski, B. Heinold and I. Tegen, Interannual variability in the Saharan dust source activation—Toward understanding the differences between 2007 and 2008, *Journal of Geophysical Research: Atmospheres*, 2016, **121**, 4538-4562.
4. A. E. Barkley, A. Pourmand, J. Longman, A. Sharifi, J. M. Prospero, K. Panechou, N. Bakker, N. Drake, D. Guinoiseau and C. J. Gaston, Interannual variability in the source location of north African dust transported to the Amazon, *Geophysical research letters*, 2022, **49**, e2021GL097344.
5. S. Alonso-Pérez, E. Cuevas, X. Querol, J. C. Guerra and C. Pérez, African dust source regions for observed dust outbreaks over the Subtropical Eastern North Atlantic region, above 25 N, *Journal of Arid Environments*, 2012, **78**, 100-109.
6. I. Ashpole and R. Washington, Intraseasonal variability and atmospheric controls on daily dust occurrence frequency over the central and western Sahara during the boreal summer, *Journal of Geophysical Research: Atmospheres*, 2013, **118**, 12,915-912,926.
7. S. Rodríguez, E. Cuevas, J. Prospero, A. Alastuey, X. Querol, J. López-Solano, M. García and S. Alonso-Pérez, Modulation of Saharan dust export by the North African dipole, *Atmospheric Chemistry and Physics*, 2015, **15**, 7471-7486.
8. R. M. Harrison, A. M. Jones, P. D. Biggins, N. Pomeroy, C. S. Cox, S. P. Kidd, J. L. Hobman, N. L. Brown and A. Beswick, Climate factors influencing bacterial count in background air samples, *International journal of biometeorology*, 2005, **49**, 167-178.
9. Y. Li, J. T. Randerson, N. M. Mahowald and P. J. Lawrence, Deforestation strengthens atmospheric transport of mineral dust and phosphorus from North Africa to the Amazon, *Journal of Climate*, 2021, **34**, 6087-6096.
10. P. Knippertz and M. C. Todd, Mineral dust aerosols over the Sahara: Meteorological controls on emission and transport and implications for modeling, *Reviews of Geophysics*, 2012, **50**.
11. I. Koren, Y. J. Kaufman, R. Washington, M. C. Todd, Y. Rudich, J. V. Martins and D. Rosenfeld, The Bodélé depression: a single spot in the Sahara that provides most of the mineral dust to the Amazon forest, *Environmental Research Letters*, 2006, **1**, 014005.
12. W. Abouchami, K. Näthe, A. Kumar, S. J. Galer, K. P. Jochum, E. Williams, A. M. Horbe, J. W. Rosa, W. Balsam and D. Adams, Geochemical and isotopic characterization of the Bodélé Depression dust source and implications for transatlantic dust transport to the Amazon Basin, *Earth and Planetary Science Letters*, 2013, **380**, 112-123.
13. A. Pourmand, J. M. Prospero and A. Sharifi, Geochemical fingerprinting of trans-Atlantic African dust based on radiogenic Sr-Nd-Hf isotopes and rare earth element anomalies, *Geology*, 2014, **42**, 675-678.

14. A. Kumar, W. Abouchami, S. Galer, S. P. Singh, K. Fomba, J. Prospero and M. O. Andreae, Seasonal radiogenic isotopic variability of the African dust outflow to the tropical Atlantic Ocean and across to the Caribbean, *Earth and Planetary Science Letters*, 2018, **487**, 94-105.
15. J. Favet, A. Lapanje, A. Giongo, S. Kennedy, Y.-Y. Aung, A. Cattaneo, A. G. Davis-Richardson, C. T. Brown, R. Kort and H.-J. Brumsack, Microbial hitchhikers on intercontinental dust: catching a lift in Chad, *The ISME journal*, 2013, **7**, 850-867.
16. A. Stohl, Computation, accuracy and applications of trajectories—A review and bibliography, *Atmospheric Environment*, 1998, **32**, 947-966.
17. U. Kulshrestha and B. Kumar, Airmass trajectories and long range transport of pollutants: review of wet deposition scenario in South Asia, *Advances in Meteorology*, 2014, **2014**, 596041.
18. J. Hegarty, R. R. Draxler, A. F. Stein, J. Brioude, M. Mountain, J. Eluszkiewicz, T. Nehrkorn, F. Ngan and A. Andrews, Evaluation of Lagrangian particle dispersion models with measurements from controlled tracer releases, *Journal of Applied Meteorology and Climatology*, 2013, **52**, 2623-2637.
19. T. Chai, A. Stein and F. Ngan, Weak-constraint inverse modeling using HYSPLIT-4 Lagrangian dispersion model and Cross-Appalachian Tracer Experiment (CAPTEX) observations–effect of including model uncertainties on source term estimation, *Geoscientific Model Development*, 2018, **11**, 5135-5148.
20. K. A. Gebhart, B. A. Schichtel and M. G. Barna, Directional biases in back trajectories caused by model and input data, *Journal of the Air & Waste Management Association*, 2005, **55**, 1649-1662.
21. H. L. Cassol, L. G. Domingues, A. H. Sanchez, L. S. Basso, L. Marani, G. Tejada, E. Arai, C. Correia, C. B. Alden and J. B. Miller, Determination of region of influence obtained by aircraft vertical profiles using the density of trajectories from the HYSPLIT model, *Atmosphere*, 2020, **11**, 1073.
22. H. E. Fuelberg, R. O. Loring Jr, M. V. Watson, M. Sinha, K. E. Pickering, A. M. Thompson, G. W. Sachse, D. R. Blake and M. R. Schoeberl, TRACE A trajectory intercomparison: 2. Isentropic and kinematic methods, *Journal of Geophysical Research: Atmospheres*, 1996, **101**, 23927-23939.